

Research Article

Numerical Simulation of a Class of Three-Dimensional Kolmogorov Model with Chaotic Dynamic Behavior by Using Barycentric Interpolation Collocation Method

Mingjing Du ¹, Junmei Li ², Yulan Wang ², and Wei Zhang ³

¹Institute of Computer Information Management, Inner Mongolia University of Finance and Economics, Hohhot 010070, China

²Department of Mathematics, Inner Mongolia University of Technology, Hohhot 010051, China

³Institute of Economics and Management, Jining Normal University, Jining 012000, Inner Mongolia, China

Correspondence should be addressed to Wei Zhang; jnsfxyzw@163.com

Received 5 January 2019; Revised 13 February 2019; Accepted 3 March 2019; Published 9 April 2019

Academic Editor: Giacomo Innocenti

Copyright © 2019 Mingjing Du et al. This is an open access article distributed under the Creative Commons Attribution License, which permits unrestricted use, distribution, and reproduction in any medium, provided the original work is properly cited.

This paper numerically simulates three-dimensional Kolmogorov model with chaotic dynamic behavior by barycentric Lagrange interpolation collocation method. Some numerical examples are studied for finding some new chaotic behaviors and demonstrating some existing chaotic dynamic behaviors of the Kolmogorov model. Results obtained by the present method indicate that the method has merits of small operations and good numerical stability.

1. Introduction

J.P. Berrut [1, 2] introduced barycentric Lagrange interpolation and studied its numerical stability and convergence. Barycentric Lagrange interpolation is unconditionally stable at the Chebyshev points. S.P. Li, Z.Q. Wang [3, 4] gave some algorithms of barycentric Lagrange interpolation collocation method (BLICM). Some authors [3, 5–8] solved all sorts of equations and showed the BLICM has merits of small operations and high precision (see [3, 4, 9]). This paper numerically simulates some three-dimensional Kolmogorov models with chaotic dynamic behavior. The purpose of this paper is to find some new chaotic behaviors and verify the existing chaotic dynamic behaviors by the BLICM.

Three-dimensional Kolmogorov models comprise a significant class of ecological models that are used widely in ecology to represent the dynamic behavior of prey and predators, which are expressed in the following form:

$$\frac{dx}{dt} = xf_1(x, y, z),$$

$$\frac{dy}{dt} = yf_2(x, y, z),$$

$$\frac{dz}{dt} = zf_3(x, y, z),$$

$$x, y, z \geq 0, \quad 0 \leq t \leq T,$$

(1)

where x, y, z represents the population density of the species and $f_i(x, y, z)$ represents the per capita growth rate of the x, y, z species.

In ecology, the most frequently used model is the Lotka-Volterra system; that is, each per capita growth function f_i is affine and chosen as the logistic growth. In this circumstance, model (1) reads as

$$\frac{dx}{dt} = x(r_1 - a_{11}x - a_{12}y - a_{13}z),$$

$$\frac{dy}{dt} = y(r_2 - a_{21}x - a_{22}y - a_{23}z),$$

$$\frac{dz}{dt} = z(r_3 - a_{31}x - a_{32}y - a_{33}z).$$

(2)

$$x, y, z \geq 0, \quad 0 \leq t \leq T,$$

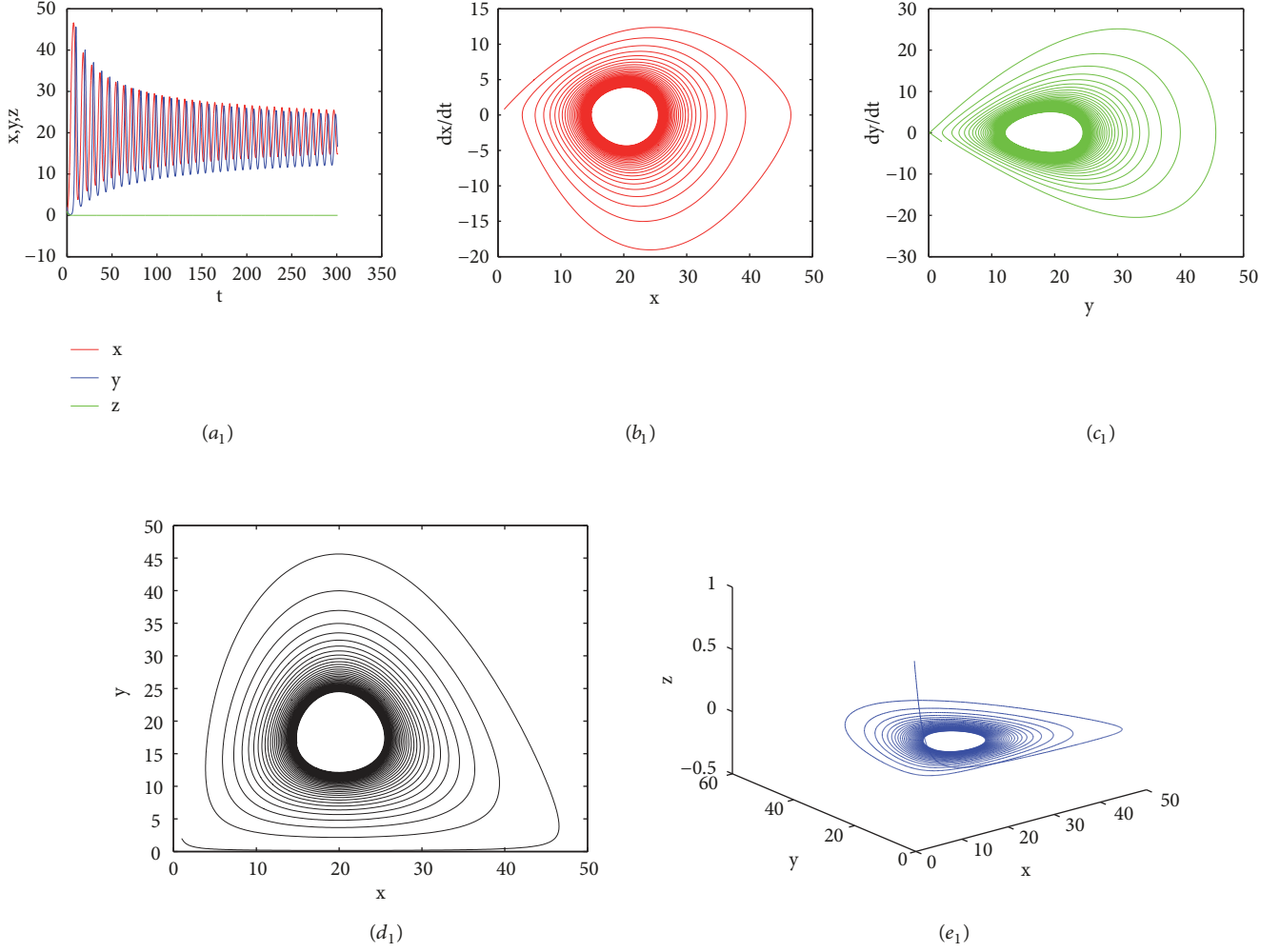


FIGURE 1: The three species food chain model for Experiment 1 with $r = 1$: (a₁) time series plot; (b₁) phase diagram of x ; (c₁) phase diagram of y ; (d₁) projected on the (x, y) -plane; (e₁) on the three-dimensional space.

Model (2) is a totally competitive system if all parameters r_i, a_{ij} are positive.

There are several famous functional responses in the Kolmogorov model which are referred to as Holling type I, type II, type III, type IV, Monod-Haldane type, Hassel-Verley type, Beddington-DeAngelis type functional response, etc.

In this paper, we consider the following three-dimensional Kolmogorov model with functional response:

$$\begin{aligned} \frac{dx}{dt} &= x(r_1 - a_{11}x - a_{12}y - a_{13}z) + h_1(x, y, z), \\ \frac{dy}{dt} &= y(r_2 - a_{21}x - a_{22}y - a_{23}z) + h_2(x, y, z), \\ \frac{dz}{dt} &= z(r_3 - a_{31}x - a_{32}y - a_{33}z) + h_3(x, y, z), \end{aligned} \quad (3)$$

$$x, y, z \geq 0, \quad 0 \leq t \leq T,$$

with the following initial condition:

$$x(0) = c_1,$$

$$y(0) = c_2,$$

$$z(0) = c_3,$$

(4)

where x, y, z represent the population density of the species and $h_i(x, y, z)$ is the known functional response. r_i, c_i, a_{ij} are known constants. x, y, z are unknown functions of time t .

Many researchers [10–20] studied the dynamics of three dimensional Kolmogorov model with different type of functional response in theory. They found some chaotic dynamics [13, 18–23] of the three-dimensional Kolmogorov model. Chaos and hyperchaos exist in many natural processes and are one of the main contents of nonlinear science research. Although many kinds of numerical methods of the Kolmogorov model have been announced, simple and efficient methods have always been the direction that scholars strive to pursue. This paper suggests the BLICM to solve the three-dimensional Kolmogorov model. Model (3) is adopted as an example to elucidate the solution process.

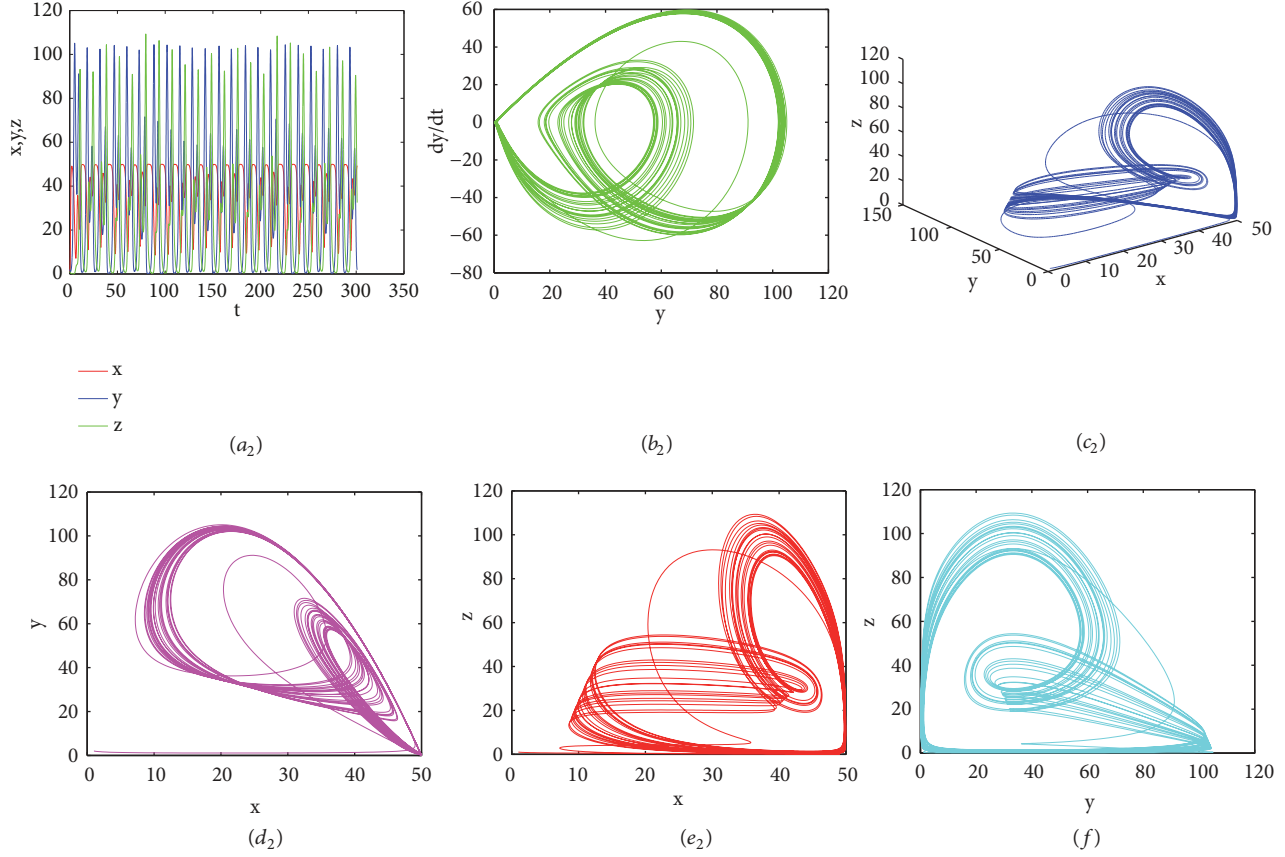


FIGURE 2: The three-species food chain model for Experiment 1 with $r = 4.2$: (a₂) time series plot; (b₂) phase diagram of y ; (c₂) on the three-dimensional space; (d₂) projected on the (x, y) -plane; (e₂) projected on the (x, z) -plane; (f) projected on the (y, z) -plane.

2. Barycentric Lagrange Interpolation Collocation Method

First of all, we discrete computational interval $[0, T]$ by Chebyshev points into $0 = t_1 < t_2 < \dots < t_M = T$ and construct following linear iterative format of model (3):

$$\begin{aligned} \frac{dx_n}{dt} &= r_1 x_n - (a_{11} x_n + a_{12} y_n + a_{13} z_n) x_{n-1} \\ &\quad + h_1(x_{n-1}, y_{n-1}, z_{n-1}), \\ \frac{dy_n}{dt} &= r_2 y_n - (a_{21} x_n + a_{22} y_n + a_{23} z_n) y_{n-1} \end{aligned}$$

$$\begin{aligned} &+ h_2(x_{n-1}, y_{n-1}, z_{n-1}), \\ \frac{dz_n}{dt} &= r_3 z_n - (a_{31} x_n + a_{32} y_n + a_{33} z_n) z_{n-1} \\ &+ h_3(x_{n-1}, y_{n-1}, z_{n-1}). \end{aligned} \quad (5)$$

The format (5) is convergent; then $x_n(t) \rightarrow x(t)$, $y_n(t) \rightarrow y(t)$, $z_n(t) \rightarrow z(t)$, ($n \rightarrow \infty$).

Next, we transform format (5) into the following linear algebraic equations.

$$\begin{bmatrix} D - r_1 I + a_{11} \text{diag}(x_{n-1}) & a_{12} \text{diag}(x_{n-1}) & a_{13} \text{diag}(x_{n-1}) \\ a_{21} \text{diag}(y_{n-1}) & D - r_2 I + a_{22} \text{diag}(y_{n-1}) & a_{23} \text{diag}(y_{n-1}) \\ a_{31} \text{diag}(z_{n-1}) & a_{32} \text{diag}(z_{n-1}) & D - r_3 I + a_{33} \text{diag}(z_{n-1}) \end{bmatrix} \begin{bmatrix} x_n \\ y_n \\ z_n \end{bmatrix} = \begin{bmatrix} h_1(x_{n-1}, y_{n-1}, z_{n-1}) \\ h_2(x_{n-1}, y_{n-1}, z_{n-1}) \\ h_3(x_{n-1}, y_{n-1}, z_{n-1}) \end{bmatrix} \quad (6)$$

where $D = (\xi_j^i(t_i))_{i,j=1,2,\dots,M}$ is M order matrix. I is M order unit matrix and diag is a symbol of diagonal matrix

composed of vectors. $\xi_j(t) = (\omega_j/(t - t_j)) / \sum_{k=1}^M (\omega_k/(t - t_k))$ is, respectively, barycentric interpolation primary function

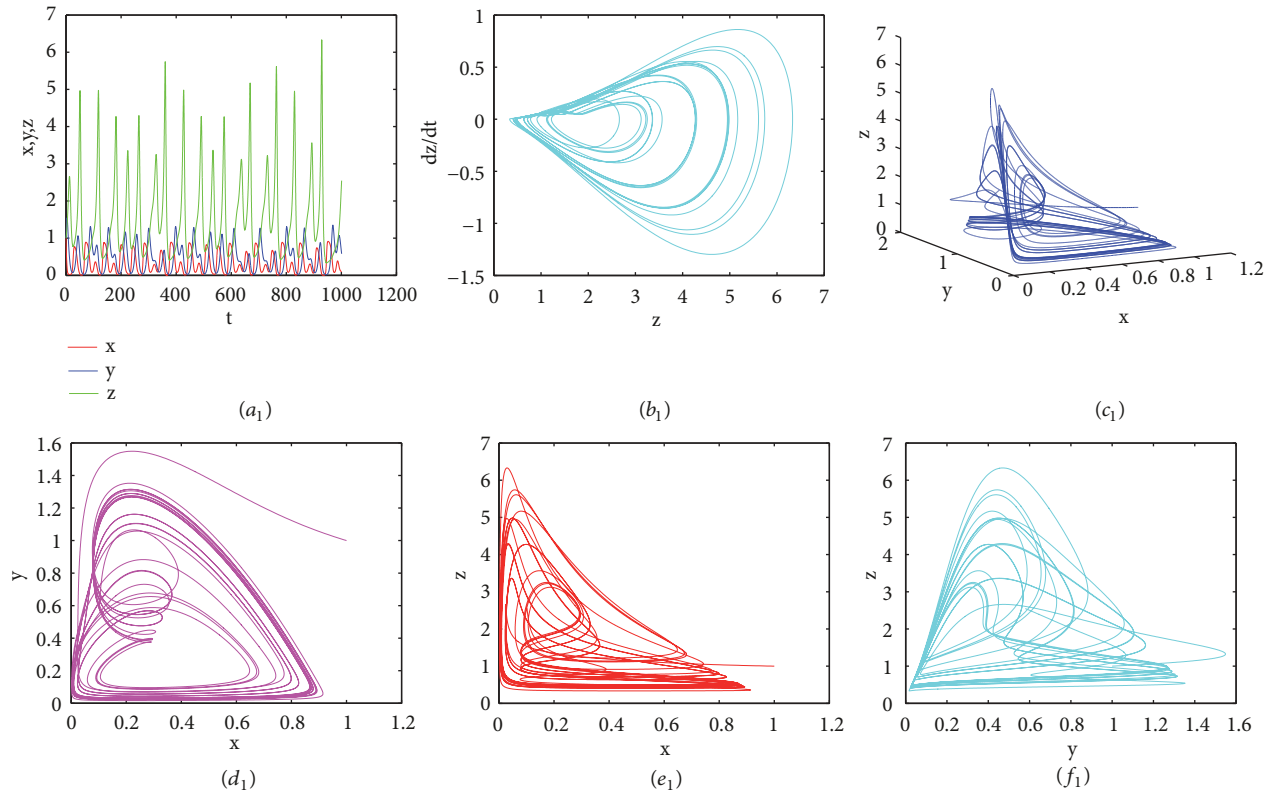


FIGURE 3: A tritrophic food web system for Experiment 2 with the initial condition (1): (a₁) time series plot of x, y, z ; (b₁) phase diagram of z ; (c₁) on the three-dimensional space; (d₁) projected on the (x, y) -plane; (e₁) projected on the (x, z) -plane; (f₁) projected on the (y, z) -plane.

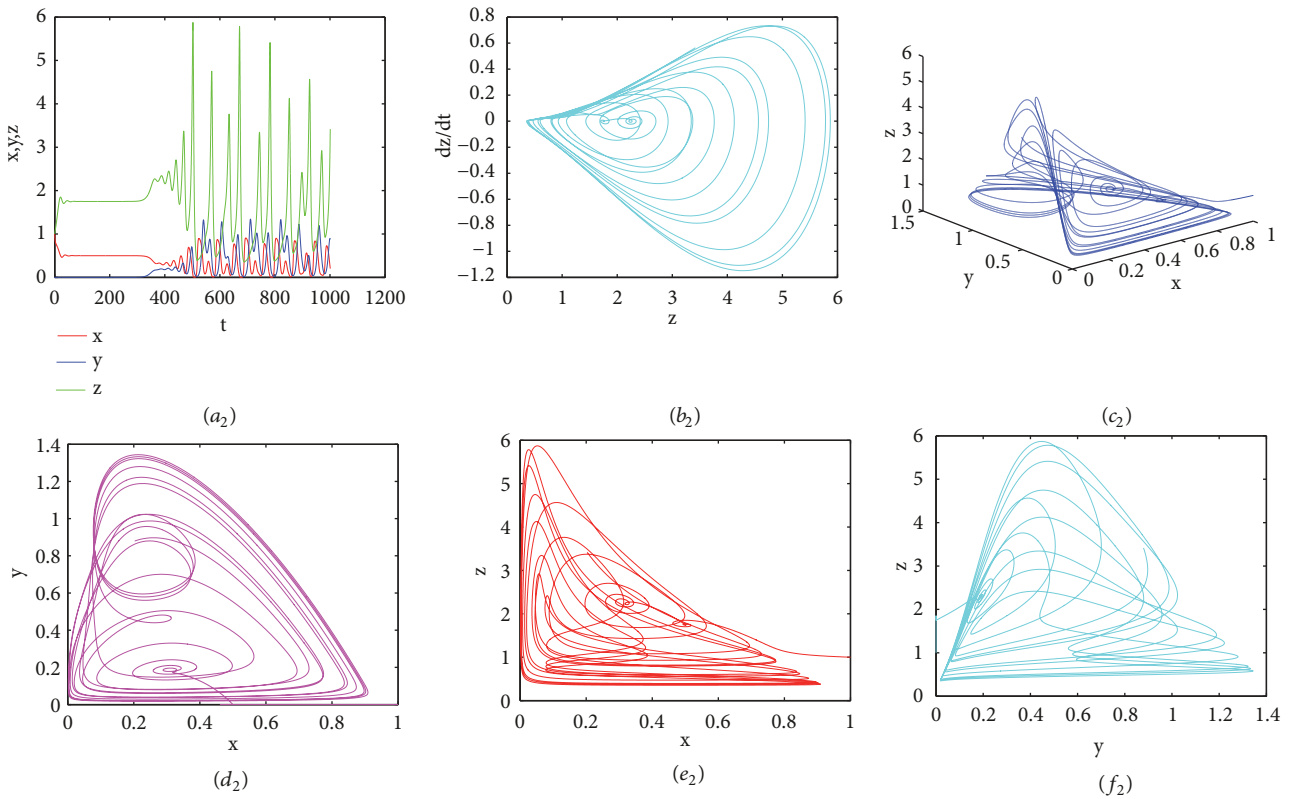


FIGURE 4: A tritrophic food web system for Experiment 2 with the initial condition (2): (a₂) time series plot of x, y, z ; (b₂) phase diagram of z ; (c₂) on the three-dimensional space; (d₂) projected on the (x, y) -plane; (e₂) projected on the (x, z) -plane; (f₂) projected on the (y, z) -plane.

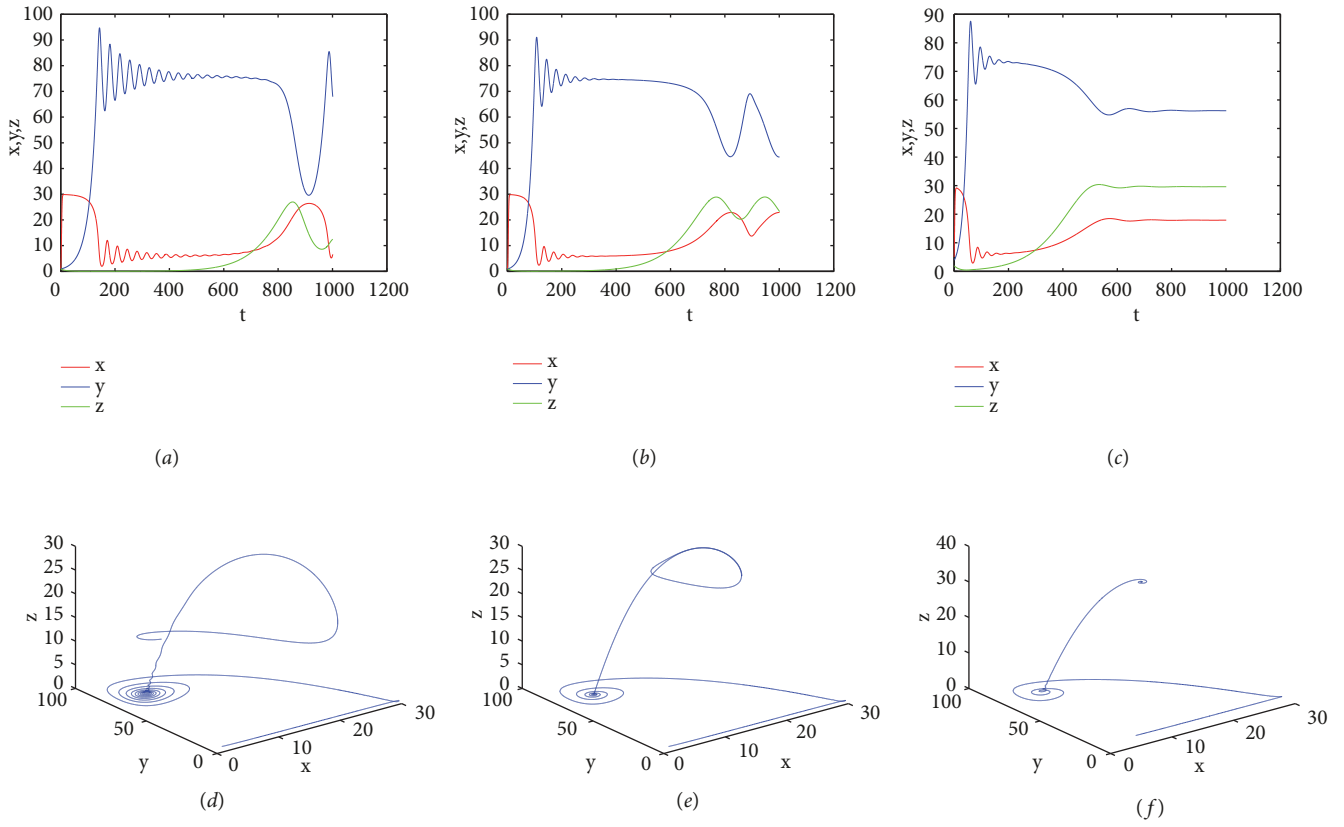


FIGURE 5: Time series plots and the three-dimensional space graphs of the tritrophic food chain model for Experiment 3 with different parameters: (a) and (d) $j = 7$; (b) and (e) $j = 9$; (c) and (f) $j = 12$.

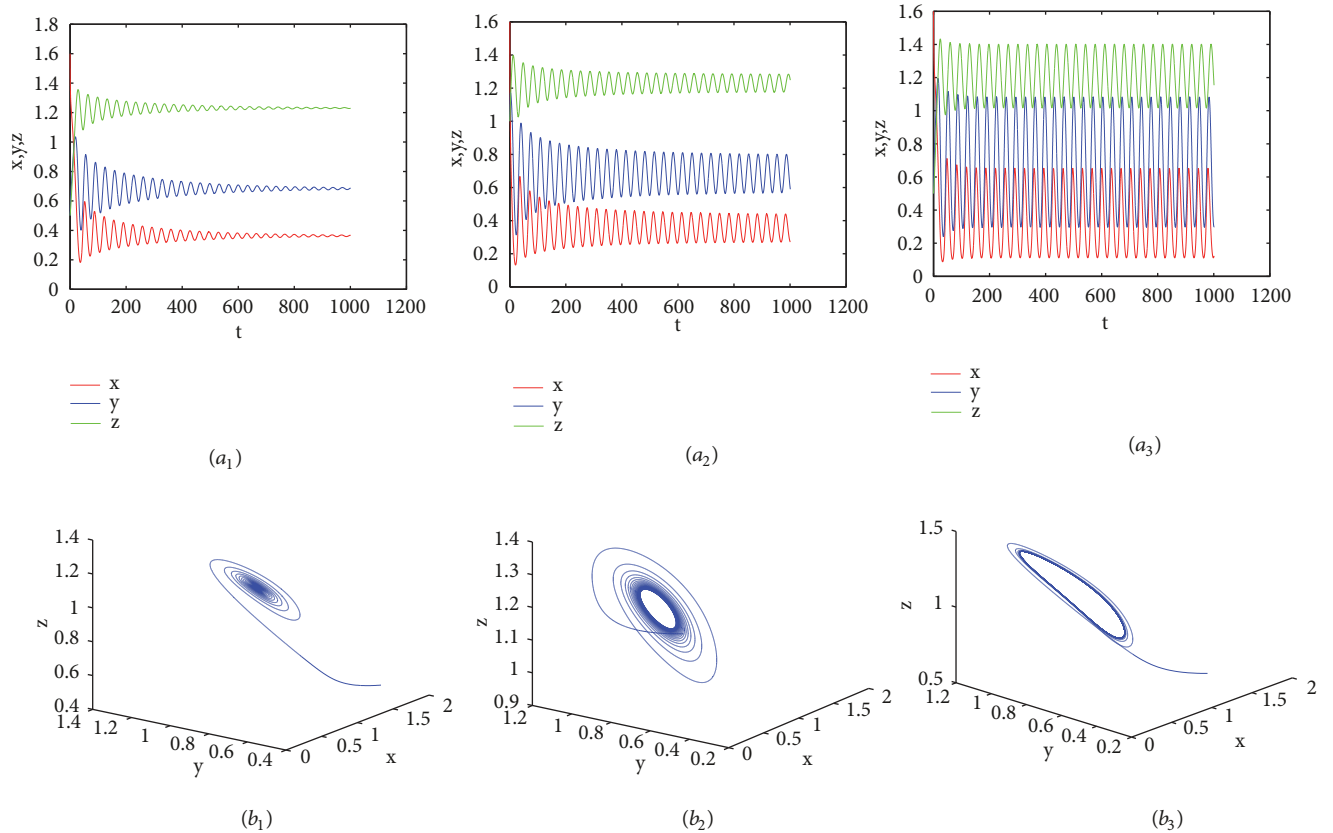


FIGURE 6: Time series plots and the three-dimensional space graphs of Experiment 4 with different parameters: (a₁) and (b₁) $k_1 = 0.958$; (a₂) and (b₂) $k_1 = 0.989$; (a₃) and (b₃) $k_1 = 1.089$.

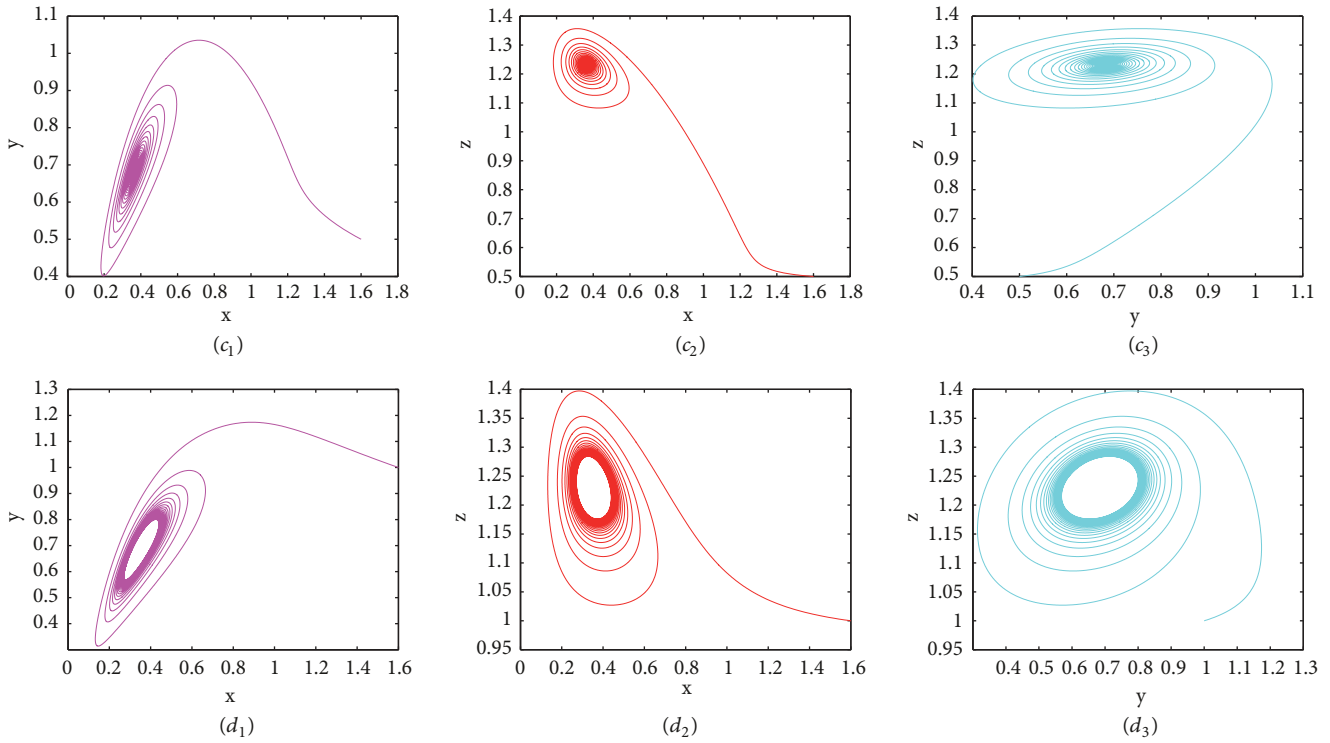


FIGURE 7: The results of Experiment 4: (c_i) with $k_1 = 0.958$ and (d_i) with $k_1 = 0.989 (i = 1, 2, 3)$, (c_1) and (d_1) projected on the (x, y) -plane; (c_2) and (d_2) projected on the (x, z) -plane; (c_3) and (d_3) projected on the (y, z) -plane.

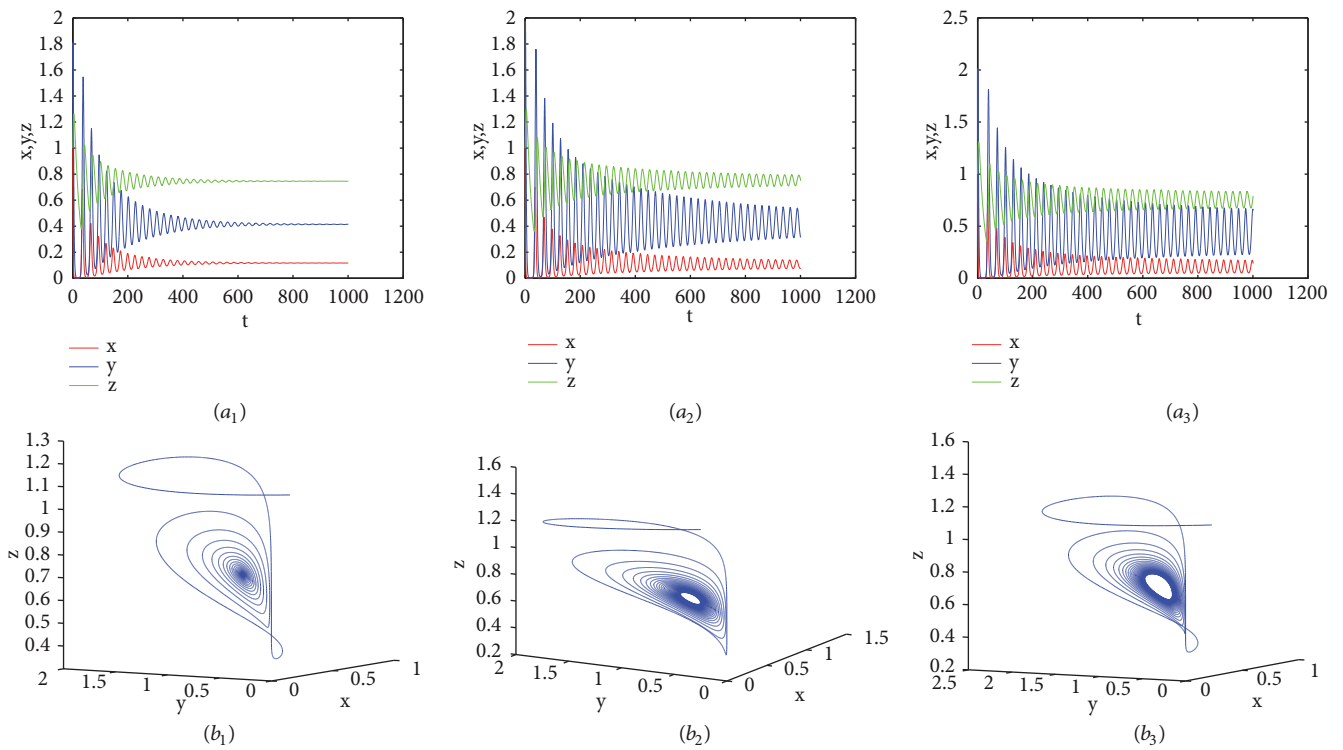


FIGURE 8: Time series plots and the three-dimensional space graphs of Experiment 5 with different parameters: (a_1) and (b_1) $c = 1.4$; (a_2) and (b_2) $c = 1.575$; (a_3) and (b_3) $c = 1.62$.

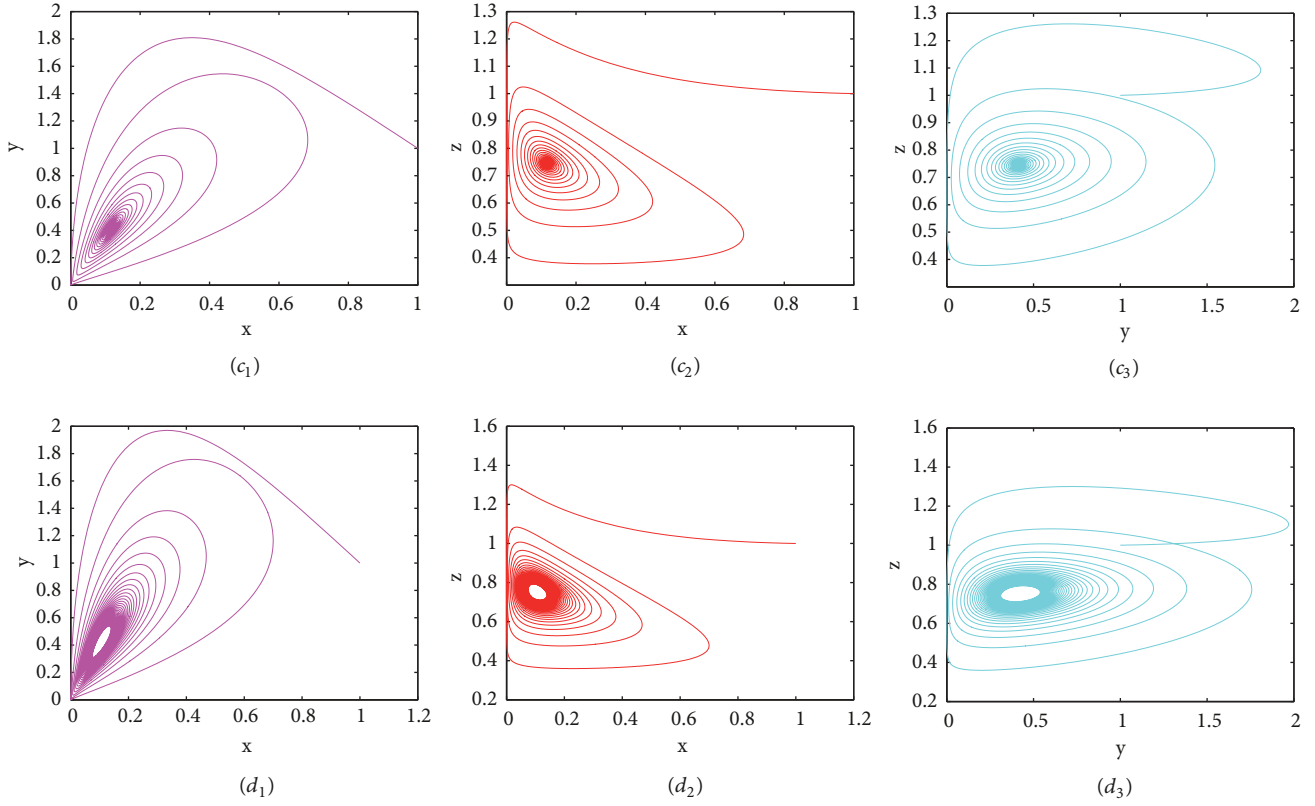


FIGURE 9: The results of Experiment 5: (c_i) with $c = 1.4$ and (d_i) with $c = 1.575$ ($i = 1, 2, 3$), (c_1) and (d_1) projected on the (x, y) -plane; (c_2) and (d_2) projected on the (x, z) -plane; (c_3) and (d_3) projected on the (y, z) -plane.

and $\omega_j = 1/\prod_{i=1, j \neq k}^M (t_i - t_j)$ is center of gravity Lagrange interpolation weight. The vector

$$[x_n, y_n, z_n] = [x_n(t_1), x_n(t_2), \dots, x_n(t_M), y_n(t_1), y_n(t_2), \dots, y_n(t_M), z_n(t_1), z_n(t_2), \dots, z_n(t_M)]. \quad (7)$$

The vector

$$\begin{aligned} & [h_1(x_{n-1}, y_{n-1}, z_{n-1}), h_2(x_{n-1}, y_{n-1}, z_{n-1}), \\ & h_3(x_{n-1}, y_{n-1}, z_{n-1})] \\ & = [h_1(x_{n-1}(t_1), y_{n-1}(t_1), z_{n-1}(t_1)), \dots, \\ & h_1(x_{n-1}(t_M), y_{n-1}(t_M), z_{n-1}(t_M)), \\ & h_2(x_{n-1}(t_1), y_{n-1}(t_1), z_{n-1}(t_1)), \dots, \\ & h_2(x_{n-1}(t_M), y_{n-1}(t_M), z_{n-1}(t_M)), \\ & h_3(x_{n-1}(t_1), y_{n-1}(t_1), z_{n-1}(t_1)), \dots, \\ & h_3(x_{n-1}(t_M), y_{n-1}(t_M), z_{n-1}(t_M))]. \end{aligned} \quad (8)$$

The last and the first line of equations (6) are replaced separately by the equation of the initial condition (9) in turn.

$$\begin{aligned} \sum_{i=1}^M \xi_i(0) x_n(t_i) &= c_1, \\ \sum_{i=1}^M \xi_i(0) y_n(t_i) &= c_2, \\ \sum_{i=1}^M \xi_i(0) z_n(t_i) &= c_3. \end{aligned} \quad (9)$$

So, we can get a numerical solution of (3) and (4).

3. Numerical Experiments

In this section, some numerical examples are studied to demonstrate the accuracy of the present method. The examples are computed using MatlabR2017a. In numerical experiments, the number of nodes $M = 40$. The accuracy of iteration control $\varepsilon = 10^{-10}$ and the initial iteration value $x_0 = y_0 = z_0 = 0; x_1 = y_1 = z_1 = t$.

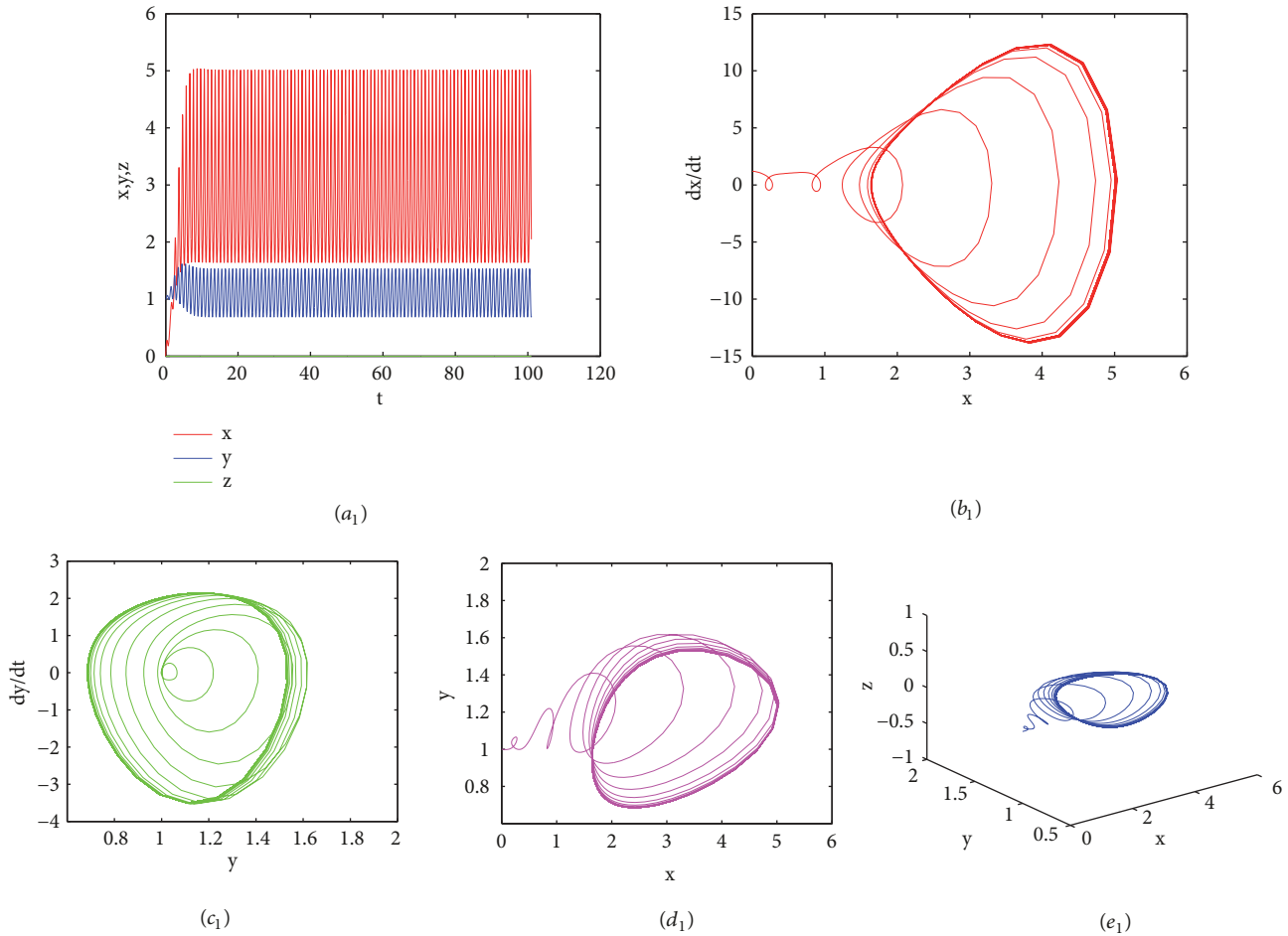


FIGURE 10: The results of Experiment 6: (a₁) time series plot of x, y, z ; (b₁) phase diagram of x ; (c₁) phase diagram of y ; (d₁) projected on the (x, y) -plane; (e₁) on the three-dimensional space.

Experiment 1. We consider the following three-species food chain model [18]:

$$\begin{aligned} \dot{x} &= rx \left(1 - \frac{x}{50} \right) - \frac{0.1xy}{1 + 0.1x}, \\ \dot{y} &= -y + 0.05xy - \frac{0.1yz}{1 + 0.2y}, \\ \dot{z} &= -z + 0.03yz, \end{aligned} \quad (10)$$

where r is real parameters, which satisfy the initial condition $x(0) = 1, y(0) = 2, z(0) = 1$. Results of Experiment 1 are given in Figures 1-2.

Figure 1 is obtained by using the current method with $r = 1$. Among them, (a₁) is the time series plot; (b₁) is the phase diagram of x ; (c₁) is the phase diagram of y ; (d₁) is the graph projected on (x, y) -plane; (e₁) is the three-dimensional space graph. Figure 2 is obtained by using the current method with $r = 4.2$. (a₂) is the time series plot; (b₂) is the phase diagram of y ; (c₂) is the three-dimensional space graph; (d₂) is the graph projected on (x, y) -plane; (e₂) is the the graph projected on (x, z) -plane; (f) is the graph projected on (y, z) -plane.

Figure 1 gets some new chaotic behaviors. Figure 2 verifies the existing chaotic dynamic behaviors [18]. Our

study suggests that model (10) will go chaotic when the rate of the self-reproduction of the prey is large. Our numerical results are in good agreement with the theory [18].

Experiment 2. We consider the following tritrophic food chain model [19]:

$$\begin{aligned} \dot{x} &= x \left[1 - x - \frac{y}{1 + 1.4x} - \frac{z}{1 + 5x + 8y} \right], \\ \dot{y} &= y \left[-0.16 + \frac{x}{1 + 1.4x} - \frac{0.1z}{1 + 5x + 8y} \right], \\ \dot{z} &= 0.1z^2 - \frac{0.5z^2}{1 + 8x + 8y}, \end{aligned} \quad (11)$$

In comparison with [19], we get better numerical results; results of Experiment 2 are given in Figures 3-4. Our numerical results are in good agreement with the theory [19].

Figures 3 and 4 are obtained by using the current method with the initial conditions (1): $x(0) = 1, y(0) = 1, z(0) = 1$ and the initial conditions (2): $x(0) = 1, y(0) = 0, z(0) = 1$, respectively. (a₁) and (a₂) are the time series plot of x, y, z ; (b₁) and (b₂) are the phase diagram of z ; (c₁) and

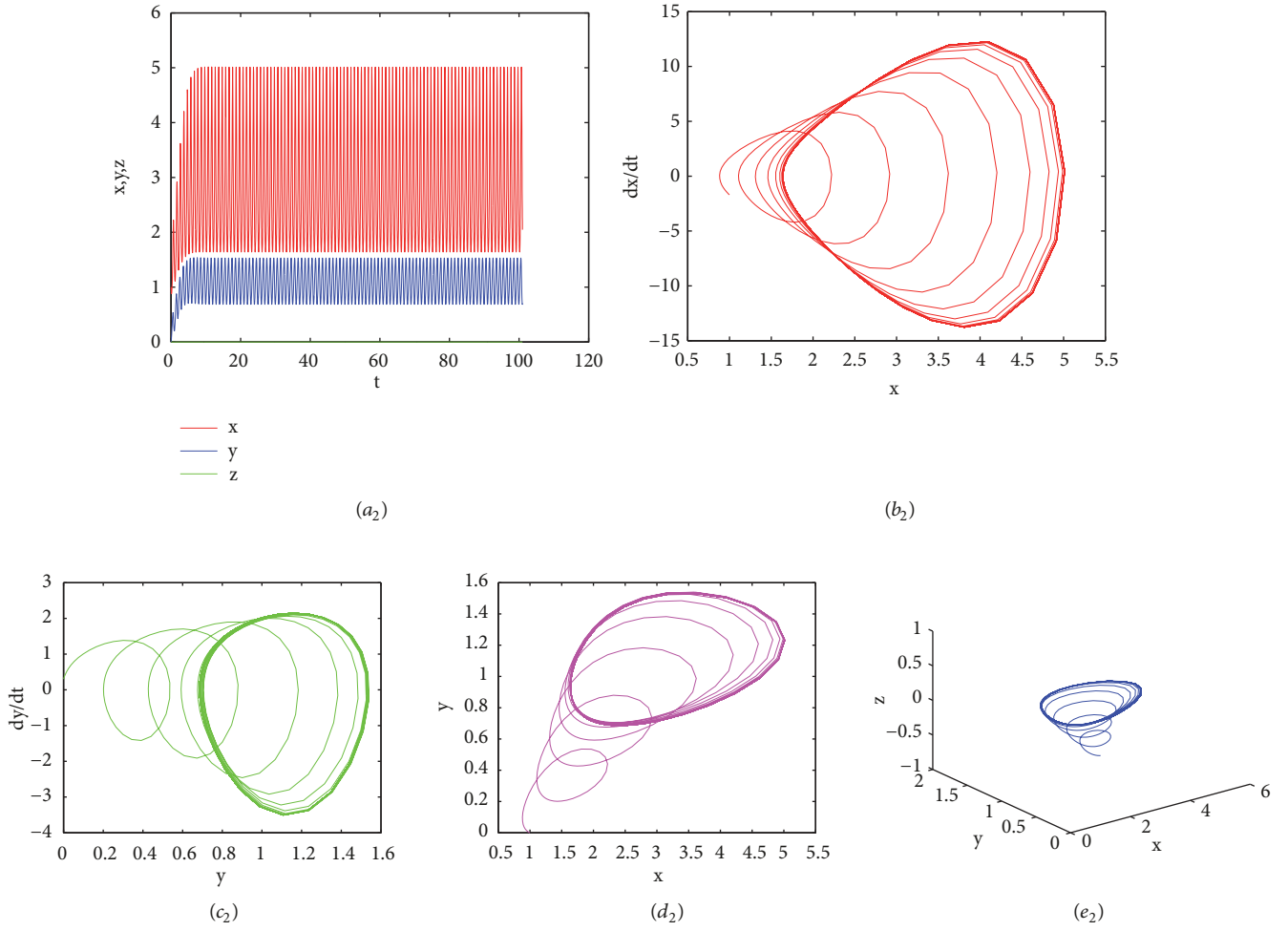


FIGURE 11: The results of Experiment 6: (a₂) time series plot of x, y, z; (b₂) phase diagram of x; (c₂) phase diagram of y; (d₂) projected on the (x, y)-plane; (e₂) on the three-dimensional space.

(c₂) are the three-dimensional space graph; (d₁) and (d₂) are the graph projected on (x, y)-plane; (e₁) and (e₂) are the graph projected on (x, z)-plane; (f₁) and (f₂) are the graph projected on (y, z)-plane. It can be seen that the change of initial conditions leads to significant changes in the time series diagrams of x, y, and z.

Experiment 3. We consider the following tritrophic food chain model [20]:

$$\begin{aligned} \dot{x} &= x \left[1 - \frac{x}{30} - \frac{wy}{x^2/a + x + 60} \right], \\ \dot{y} &= y \left[-0.05 + \frac{0.6x}{x^2/a + x + 60} - \frac{0.2z}{y + 50 + 0.21z} \right], \\ \dot{z} &= z \left[-0.06 + \frac{0.12y}{y + 50 + 0.21z} \right], \end{aligned} \quad (12)$$

where a is real parameters, which satisfy the initial condition $x(0) = 5, y(0) = 4, z(0) = 2$. Our numerical simulations and experimental results of [20] are confirmed. Results of Experiment 3 are given in Figure 5.

Figure 5 is obtained by using the current method. (a) is time series plot and (d) is the three-dimensional space graph with $a = 7$; (b) is time series plot and (e) is the three-dimensional space graph with $a = 9$; (c) is time series plot and (f) is the three-dimensional space graph with $a = 12$. We can see that, from the figure, the fluctuation range of x, y, z at $t = 900$ is very large when $a = 7$; the fluctuation range of x, y, z at $t = 900$ is obviously reduced when $a = 9$; x, y, z at $t = 900$ almost all tend to be stationary when $a = 12$.

Experiment 4. We consider the following model with Beddington-DeAngelis-type functional response [21]:

$$\begin{aligned} \dot{x} &= rx \left(1 - \frac{x}{k} \right) - \frac{axz}{1 + bx + cz}, \\ \dot{y} &= \frac{k_1 axz}{1 + bx + cz} - \alpha y - d_1 y, \\ \dot{z} &= \alpha y - d_2 z, \end{aligned} \quad (13)$$

where $r, k, a, b, c, \alpha, d_1, d_2$, and k_1 are real parameters, which satisfy the initial condition $x(0) = 1.6, y(0) = 0.5, z(0) = 0.5$. We choose the parameters $r = 1.5, k = 1.6, a = 1.4, b = 1, c =$

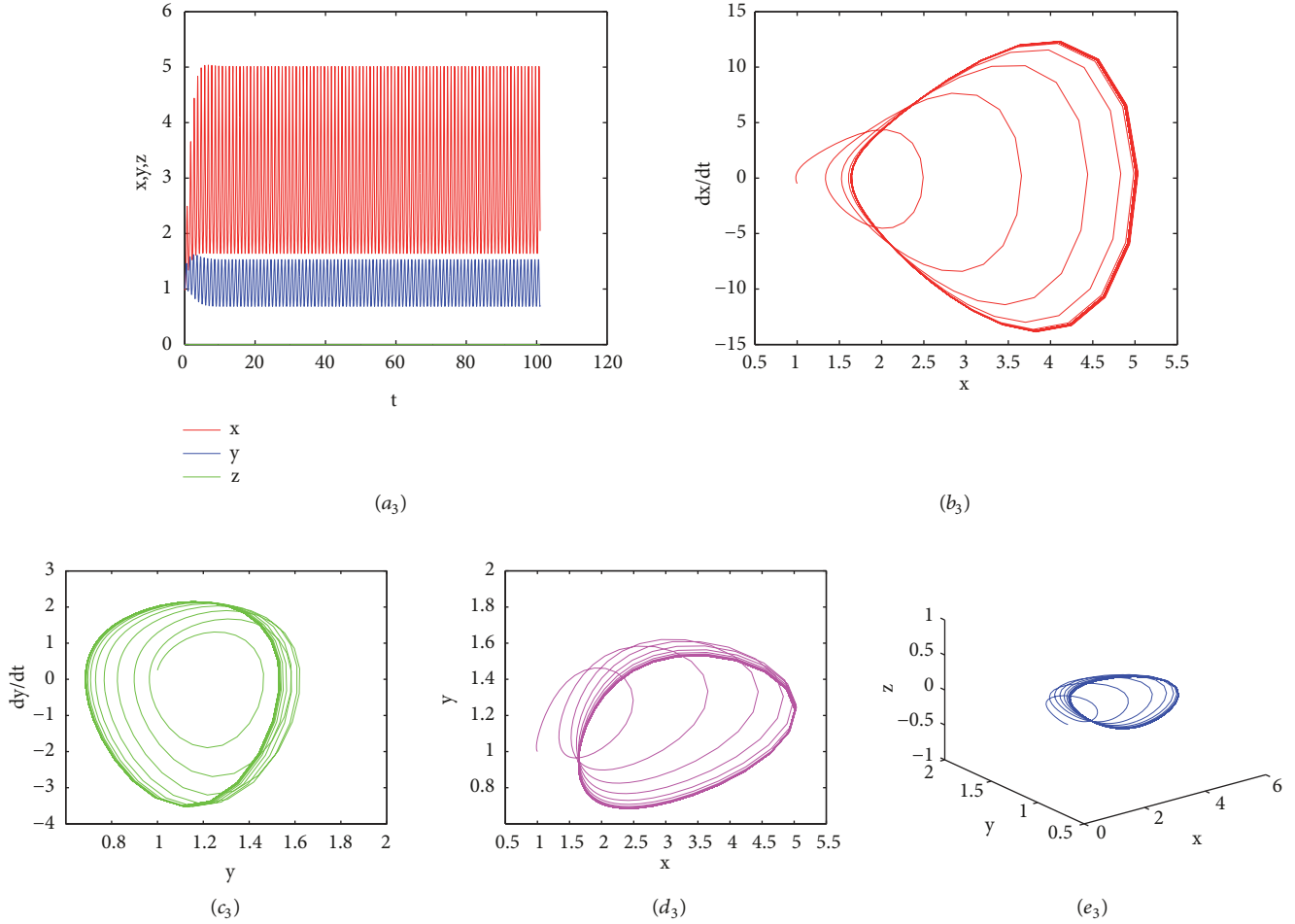


FIGURE 12: The results of Experiment 6: (a₃) time series plot of x, y, z ; (b₃) phase diagram of x ; (c₃) phase diagram of y ; (d₃) projected on the (x, y) -plane; (e₃) on the three-dimensional space.

0.1, $\alpha = 0.09, d_1 = 0.5, d_2 = 0.05$. Results of Experiment 4 are given in Figures 6-7.

Figure 6 is time series plots and the three-dimensional space graphs of a predator-prey model with Beddington-DeAngelis type functional response for Experiment 4 with different parameters obtained by using the current method. (a₁) is time series plot and (b₁) is the three-dimensional space graph with $k_1 = 0.958$; (a₂) is time series plot and (b₂) is the three-dimensional space graph with $k_1 = 0.989$; (a₃) is time series plot and (b₃) is the three-dimensional space graph with $k_1 = 1.089$. Figure 7 is obtained by using the current method with $k_1 = 0.958$ and $k_1 = 0.989$, respectively. (c₁) and (d₁) are the graph projected on (x, y) -plane; (c₂) and (d₂) are the graph projected on (x, z) -plane; (c₃) and (d₃) are the graph projected on (y, z) -plane.

Experiment 5. We consider the following model with Monod-Haldane type response function [22]:

$$\dot{x} = \rho_1 x \left(1 - \frac{x}{k_1} \right) - \frac{\beta x z}{\phi + \gamma x^2},$$

$$\dot{y} = \frac{c \beta x z}{\phi + \gamma x^2} - (\alpha + \delta_1) y,$$

$$\dot{z} = \alpha y - \delta_2 z,$$

(14)

where $\rho_1, k_1, \beta, \gamma, c, \phi, \alpha, \delta_1$, and δ_2 are real parameters, which satisfy the initial condition $x(0) = 1, y(0) = 1, z(0) = 1$. We choose the parameter $\rho_1 = 1.6, k_1 = 1.72, \beta = 1.4, \gamma = 0.01, \alpha = 0.09, \phi = 0.7, \delta_1 = 0.5, \delta_2 = 0.05$.

Our numerical simulation results are in good agreement with the theory [22]. We give some new chaotic behaviors. Results of Experiment 5 are given in Figures 8-9.

Figure 8 is time series plots and the three-dimensional space graphs of a predator-prey system with Monod-Haldane type response function for Experiment 5 with different parameters obtained by using the current method. (a₁) is time series plot and (b₁) is the three-dimensional space graph with $c = 1.4$; (a₂) is time series plot and (b₂) is the three-dimensional space graph with $c = 1.575$; (a₃) is time series plot and (b₃) is the three-dimensional space graph with $c = 1.62$. Figure 9 is obtained by using the current method with $c = 1.4$ and $c = 1.575$, respectively. (c₁) and (d₁) are

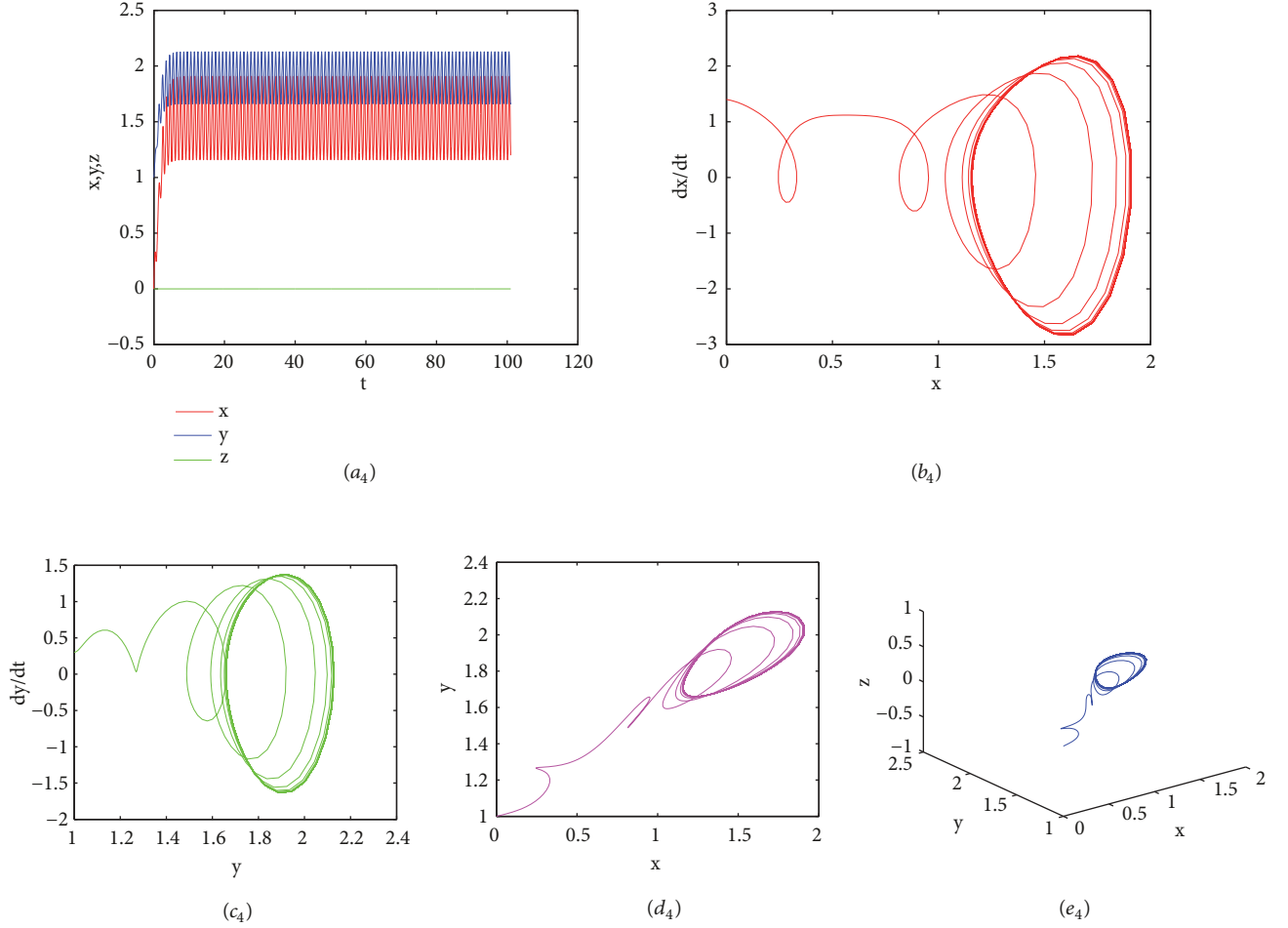


FIGURE 13: The results of Experiment 6: (a₄) time series plot of x, y, z ; (b₄) phase diagram of x ; (c₄) phase diagram of y ; (d₄) projected on the (x, y) -plane; (e₄) on the three-dimensional space.

TABLE 1: Parameters used in Experiment 6.

Figure	$b_1(t)$	$b_2(t)$	$b_3(t)$	$d_1(t)$	$d_2(t)$	$d_3(t)$	$a_1(t)$	$a_2(t)$
10, 11, 12	$0.85 + \sin(2\pi t)$	$0.75 + \sin(2\pi t)$	$0.8 + \sin(2\pi t)$	$0.35 + \cos(2\pi t)$	0.5	0.4	0.6	$0.45 + \sin(2\pi t)$
13, 14, 15	$0.45 + \sin(2\pi t)$	$0.75 + \sin(2\pi t)$	$0.8 + \sin(2\pi t)$	$0.5 + \cos(2\pi t)$	0.35	0.4	0.26	$0.3 + \sin(2\pi t)$

the graph projected on (x, y) -plane; (c₂) and (d₂) are the graph projected on (x, z) -plane; (c₃) and (d₃) are the graph projected on (y, z) -plane.

Experiment 6. We consider the following model with a Watt-type functional response [23]:

$$\begin{aligned}
 \dot{x} &= x(b_1(t) - d_1(t)x) - a_1(t)z \left(1 - \exp\left(\frac{-cx}{z^m}\right)\right) \\
 &\quad + D_1(t)(y - x), \\
 \dot{y} &= y(b_2(t) - d_2(t)y) + D_2(t)(x - y), \\
 \dot{z} &= z(b_3(t) - d_3(t)z) + a_2(t)z \left(1 - \exp\left(\frac{-cx}{z^m}\right)\right),
 \end{aligned} \tag{15}$$

Our numerical simulation results are in good agreement with the theory [23]. Compared with [23], we get better numerical results and give some new chaotic behaviors. Results of Experiment 6 are given in Figures 10–15. We choose the parameter; see Tables 1-2.

Figures 10–12 are obtained by using the current method. (a₁), (a₂), and (a₃) are the time series plot of x, y, z ; (b₁), (b₂), and (b₃) are the phase diagram of x ; (c₁), (c₂), and (c₃) are the phase diagram of y ; (d₁), (d₂), and (d₃) are the graph projected on (x, y) -plane; (e₁), (e₂), and (e₃) are the three-dimensional space graph. Figures 13–15 are obtained by using the current method. (a₄), (a₅), and (a₆) are the time series plot of x, y, z ; (b₄), (b₅), and (b₆) are the phase diagram of x ; (c₄), (c₅), and (c₆) are the phase diagram of y ; (d₄), (d₅), and (d₆) are the graph projected on (x, y) -plane; (e₄), (e₅), and (e₆) are the three-dimensional space graph.

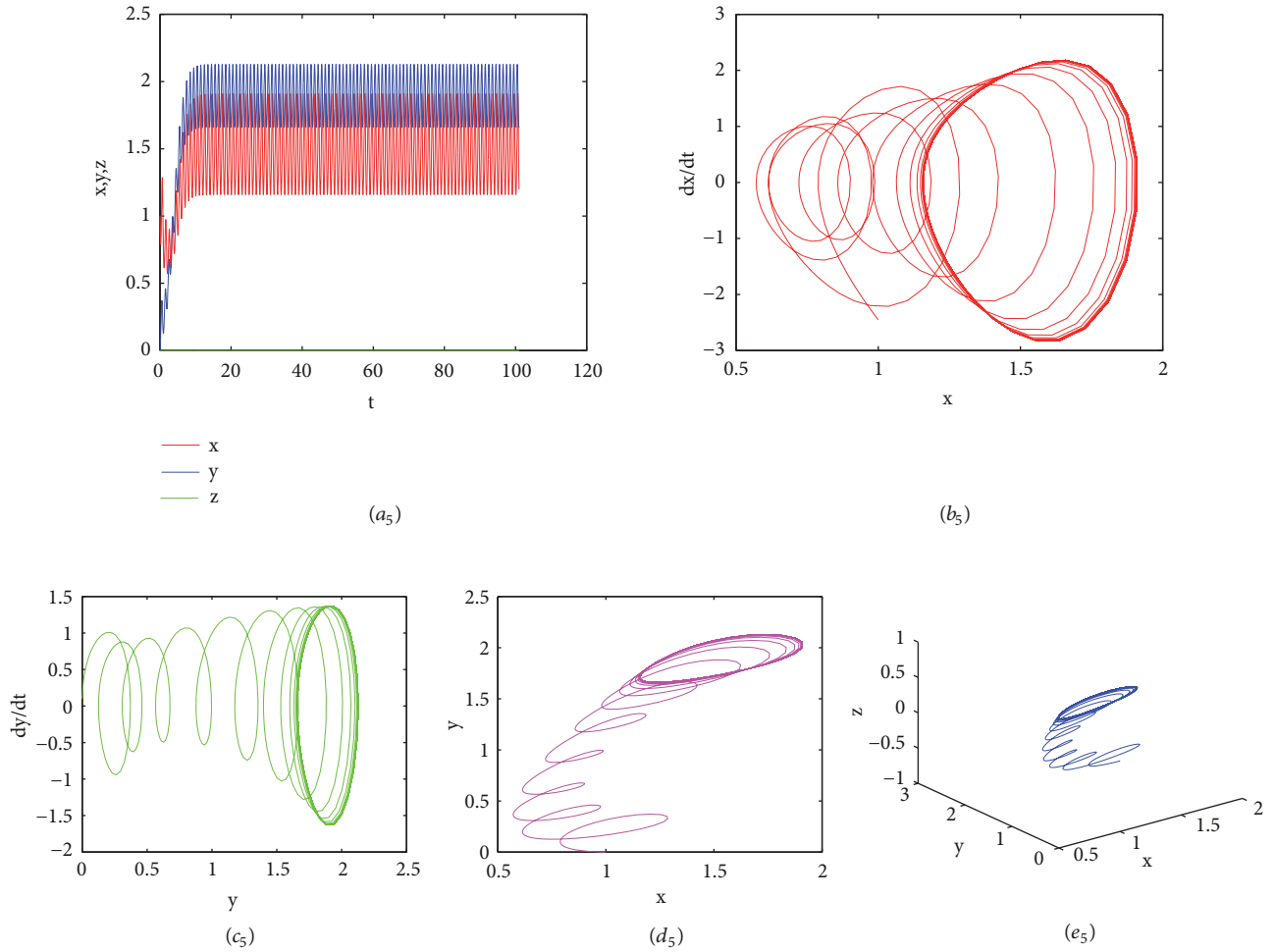


FIGURE 14: The results of Experiment 6: (a₅) time series plot of x, y, z ; (b₅) phase diagram of x ; (c₅) phase diagram of y ; (d₅) projected on the (x, y) -plane; (e₅) on the three-dimensional space.

TABLE 2: Parameters used in Experiment 6.

Figure	c	m	$D_1(t)$	$D_2(t)$	c_1	c_2	c_3
10	1	0.5	$0.2 + \cos(2\pi t)$	$0.3 + \sin(2\pi t)$	0	1	1
11	1	0.5	$0.2 + \cos(2\pi t)$	$0.3 + \sin(2\pi t)$	1	0	1
12	1	0.5	$0.2 + \cos(2\pi t)$	$0.3 + \sin(2\pi t)$	1	1	1
13	1	0.35	$0.4 + \cos(2\pi t)$	$0.1 + \sin(2\pi t)$	0	1	1
14	1	0.35	$0.4 + \cos(2\pi t)$	$0.1 + \sin(2\pi t)$	1	0	1
15	1	0.35	$0.4 + \cos(2\pi t)$	$0.1 + \sin(2\pi t)$	1	1	1

4. Conclusions and Remarks

In this paper, the three dimensional Kolmogorov model was solved by using the barycentric Lagrange interpolation collocation method. These numerical experiments illustrate that numerical results of the present method are the same as experimental results.

All computations are performed by the MatlabR2007b software packages.

Data Availability

The data used to support the findings of this study are available from the corresponding author upon request.

Conflicts of Interest

The authors declare that there are no conflicts of interest regarding the publication of this article.

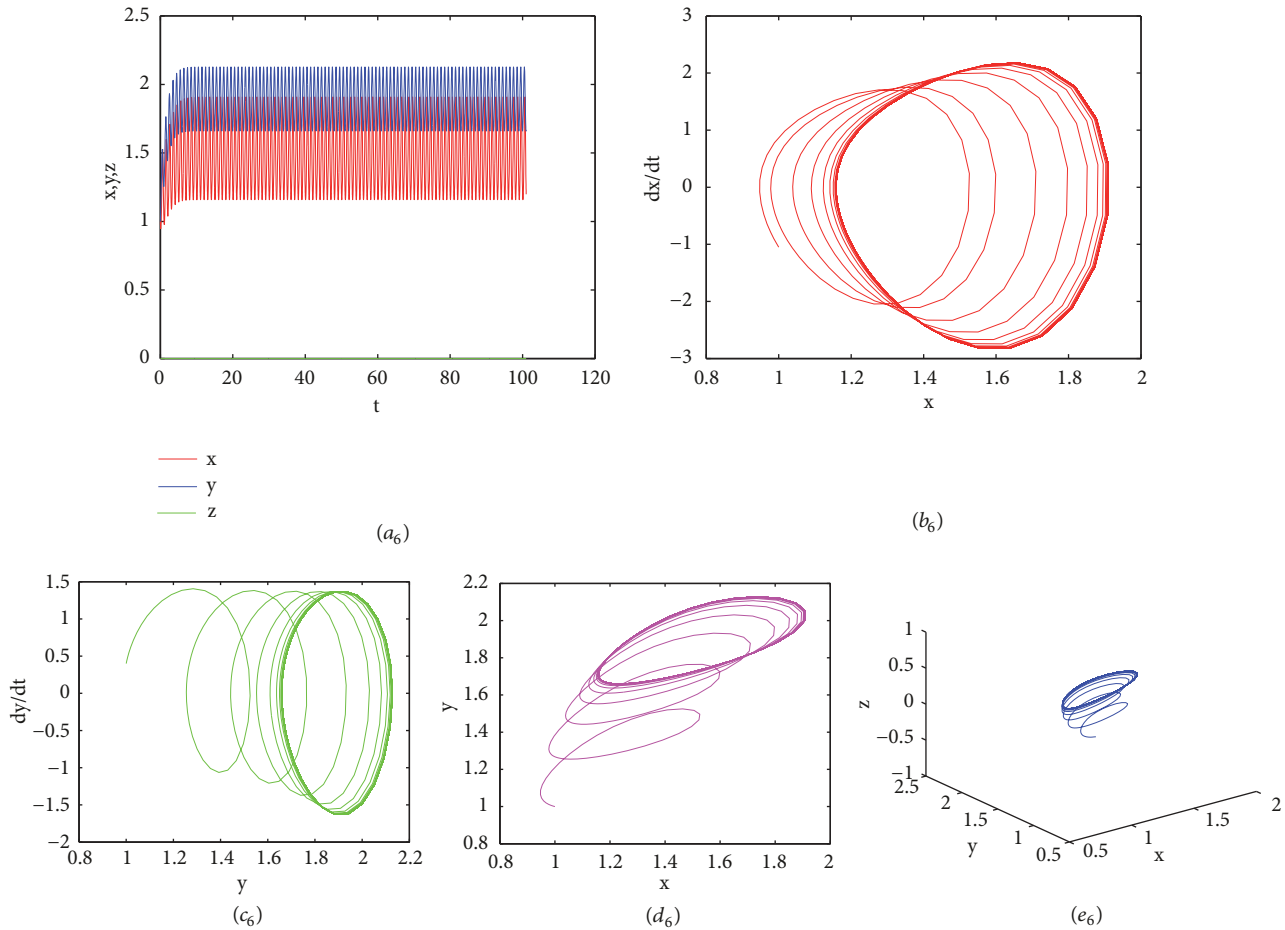


FIGURE 15: The results of Experiment 6: (a₆) time series plot of x, y, z ; (b₆) phase diagram of x ; (c₆) phase diagram of y ; (d₆) projected on the (x, y) -plane; (e₆) on the three-dimensional space.

Authors' Contributions

Mingjing Du carried out the main part of this manuscript. Wei Zhang obtained data and analyze numerical simulation results, which greatly improved the quality of the paper. Junmei Li carried out numerical simulation and gave some numerical results. Yulan Wang made the program of the barycentric interpolation collocation method in the revised version and corrected the derived results. All authors read and approved the final manuscript. When we resubmitted the revised version, we forgot to change the author list.

Acknowledgments

The authors thank the reviewers for their valuable suggestions, which greatly improved the quality of the paper. This paper is supported by the Natural Science Foundation of Inner Mongolia [2017MS0103], Inner Mongolia Maker Collaborative Innovation Center of Jining Normal University, and the National Natural Science Foundation of China [11361037].

References

- [1] J. P. Berrut and L. N. Trefethen, "Barycentric lagrange interpolation," *SIAM Review*, vol. 46, no. 3, pp. 501–517, 2004.
- [2] N. J. Higham, "The numerical stability of barycentric Lagrange interpolation," *IMA Journal of Numerical Analysis (IMAJNA)*, vol. 24, no. 4, pp. 547–556, 2004.
- [3] S. P. Li and Z. Q. Wang, *Barycentric Interpolation Collocation Method for Nonlinear Problems*, National Defense Industry Press, Beijing, China, 2015.
- [4] S. P. Li and Z. Q. Wang, *High-Precision Non-Grid Center of Gravity Interpolation Collocation Method: Algorithm, Program And Engineering Application*, Science Press, Beijing China, 2012.
- [5] H. Wu, Y. Wang, and W. Zhang, "Numerical solution of a class of nonlinear partial differential equations by using barycentric interpolation collocation method," *Mathematical Problems in Engineering*, vol. 2018, Article ID 7260346, 10 pages, 2018.
- [6] F. Liu, Y. Wang, and S. Li, "Barycentric interpolation collocation method for solving the coupled viscous Burgers' equations," *International Journal of Computer Mathematics*, vol. 95, no. 11, pp. 2162–2173, 2018.

- [7] H. Liu, J. Huang, Y. Pan, and J. Zhang, "Barycentric interpolation collocation methods for solving linear and nonlinear high-dimensional Fredholm integral equations," *Journal of Computational and Applied Mathematics*, vol. 327, pp. 141–154, 2018.
- [8] W.-H. Luo, T.-Z. Huang, X.-M. Gu, and Y. Liu, "Barycentric rational collocation methods for a class of nonlinear parabolic partial differential equations," *Applied Mathematics Letters*, vol. 68, pp. 13–19, 2017.
- [9] S. P. Li and Z. Q. Wang, "Barycentric interpolation collocation method for solving nonlinear vibration problems," *Noise Vibration Control*, vol. 28, pp. 49–52, 2018.
- [10] X. Zhang, C. Shan, Z. Jin, and H. Zhu, "Complex dynamics of epidemic models on adaptive networks," *Journal of Differential Equations*, vol. 266, no. 1, pp. 803–832, 2019.
- [11] N. Juneja and K. Agnihotri, "Conservation of a predator species in SIS prey-predator system using optimal taxation policy," *Chaos, Solitons & Fractals*, vol. 116, pp. 86–94, 2018.
- [12] R. D. Parshad, N. Kumari, A. R. Kasimov, and H. Ait Abderrahmane, "Turing patterns and long-time behavior in a three-species food-chain model," *Mathematical Biosciences*, vol. 254, pp. 83–102, 2014.
- [13] P. Paul, B. Ghosh, and T. K. Kar, "Impact of species enrichment and fishing mortality in three species food chain models," *Communications in Nonlinear Science and Numerical Simulation*, vol. 29, no. 1-3, pp. 208–223, 2015.
- [14] V. L. Kolmogorov, V. P. Fedotov, and L. F. Spevak, "A mathematical model for the formation and development of defects in metals," *Studies in Applied Mechanics*, vol. 45, no. C, pp. 51–60, 1997.
- [15] Z.-P. Ma and Y.-X. Wang, "Bifurcation of positive solutions for a three-species food chain model with diffusion," *Computers & Mathematics with Applications. An International Journal*, vol. 74, no. 12, pp. 3271–3282, 2017.
- [16] T. Zeng, Z. Teng, Z. Li, and J. Hu, "Stability in the mean of a stochastic three species food chain model with general L[formula omitted]vy jumps," *Chaos, Solitons and Fractals*, vol. 106, pp. 258–265, 2018.
- [17] S.-B. Hsu, S. Ruan, and T.-H. Yang, "Analysis of three species Lotka-Volterra food web models with omnivory," *Journal of Mathematical Analysis and Applications*, vol. 426, no. 2, pp. 659–687, 2015.
- [18] R. K. Upadhyay, "Chaotic behaviour of population dynamic systems in ecology," *Mathematical and Computer Modelling*, vol. 32, no. 9, pp. 1005–1015, 2000.
- [19] A. Priyadarshi and S. Gakkhar, "Dynamics of Leslie-Gower type generalist predator in a tri-trophic food web system," *Communications in Nonlinear Science and Numerical Simulation*, vol. 18, no. 11, pp. 3202–3218, 2013.
- [20] D. Jana, R. Agrawal, and R. K. Upadhyay, "Top-predator interference and gestation delay as determinants of the dynamics of a realistic model food chain," *Chaos, Solitons & Fractals*, vol. 69, pp. 50–63, 2014.
- [21] S. Khajanchi, "Dynamic behavior of a Beddington-DeAngelis type stage structured predator-prey model," *Applied Mathematics and Computation*, vol. 244, pp. 344–360, 2014.
- [22] S. Khajanchi, "Modeling the dynamics of stage-structure predator-prey system with Monod-Haldane type response function," *Applied Mathematics and Computation*, vol. 302, pp. 122–143, 2017.
- [23] X. Lin, Y. Jiang, and X. Wang, "Existence of periodic solutions in predator-prey with Watt-type functional response and impulsive effects," *Nonlinear Analysis. Theory, Methods & Applications. An International Multidisciplinary Journal*, vol. 73, no. 6, pp. 1684–1697, 2010.

